Exceptionally cold water days in the southern Taiwan Strait: their predictability and relation to La Niña

Yu-Hsin Cheng[1, 2], Ming-Huei Chang[1]

[1]Institute of Oceanography, National Taiwan University, Taipei, 10617, Taiwan
5 [2]State Key Laboratory of Marine Environmental Science, College of Ocean and Earth Sciences, Xiamen University, Xiamen, Fujian, China.

Correspondence to: Ming-Huei Chang (minghueichang@ntu.edu.tw)

Abstract. The objectives of this study were to assess the predictability of exceptionally cold water in the Taiwan Strait (TS) and to develop a warning system on the base of scientific mechanism, which is a component of the information technology
10 system currently under development in Taiwan to protect aquaculture against extreme hazards. Optimum interpolation sea surface temperature (SST) data were used to find exceptionally cold water days from January 1995 to May 2017. We found that the SST and wind speed over the TS are low and strong in La Niña winters, respectively. According to tests conducted using relative operating characteristic curves, predictions based on the Oceanic Niño Index and integrated wind speed can be employed at lead times of 60–210 and 0–30 days, respectively. This study utilized these two proxies to develop a possible
15 warning mechanism and concluded four colors of warning light: (1) blue, meaning normal; (2) cyan, meaning warning; (3) yellow, meaning moderate risk; and (4) red, meaning high risk. Hindcasting winters over the period 1995–2017 successfully predicted the cold water hazards in the winters of 2000, 2008, 2011, and 2012 in prior to the coldest day ~20 days..

1 Introduction

The Taiwan Strait (TS) is a northeast-to-southwest passage, with a length of 300 km and width of 180 km, from the East
20 China Sea to the South China Sea. The average depth is 50 m, and two major shallow water regions, the Taiwan Bank and Chang-Yuen Ridge, are approximately 30 m (Fig. 1). Circulation in the TS, exhibiting strong seasonal variation, is mainly dominated by monsoon forcing and topography (Jan et al. 2002). The China Coastal Current brings cold and brackish water into the northern TS during winter from December to the following January (Jan et al. 2006; Chen et al. 2016). In addition, the strong northeast monsoon reduces the northward transport of the Kuroshio Branch Current, bringing warm and saline
25 water from the western North Pacific. In summer, the southwestern monsoon replaces the northeast monsoon and dominates the circulation in the TS. During the southwest monsoon season, the northward transport is intensified and brings South China Sea water into the TS (Jan et al. 2006).

El Niño–Southern Oscillation (ENSO), which develops in the tropical Pacific and is caused by the mediation between surface wind stress and sea surface temperature (SST) variations (McPhaden et al. 2006), is an interannual climate
30 fluctuation. Although ENSO originates in the tropical Pacific, it significantly influences patterns of weather variability

worldwide, shifting the probability for droughts, floods, heat waves, severe storms and extreme events (e.g., Alexander and Scott, 2002; Philippon et al., 2012). The cold phase of ENSO, La Niña, tends to intensify the East Asian winter monsoon, which always accompanies strong northerly winds and sharp air temperature drops. By contrast, the warm phase, El Niño, suppresses the East Asian winter monsoon (Wang et al. 2000; Lau and Nath 2006). In addition, Kuo and Ho (2004) indicated

5   that the stronger northeast monsoon during a La Niña winter may modulate the sea surface currents in the TS and further cause the lower SST. For example, the southward water transport was larger and the water in the TS was generally colder in November 2000 (La Niña winter) than that in 2002 (El Niño winter). The predominance of the cold China Coastal Current, and the weakness of the warm Kuroshio Branch Current, resulted in the water temperature of the TS decreasing in the early winter of 2000 (Wu et al. 2007). By contrast, when El Niño broke out in the winter seasons from 1997 to 1998, the warm

10   water area (2°C above the regional mean) in the TS increased by 25% and nutrient concentrations decreased (Shang et al. 2005). Zhang et al. (2015) suggested that less Kuroshio water enters the southeastern TS during La Niña than El Niño events, which might modulate the interannual variability of SST in the TS. However, less severe but longer lasting phenomena, such as SST variability, may have catastrophic consequences or can be a trigger for other threats (Ustrnul et al. 2015). For example, the extreme cold or hot temperature can threaten life on earth and may even trigger a disaster (Mora and Ospina

15   2002). Previous studies have identified a correlation between local wind and circulation in the TS, and they have suggested that a La Niña winter would be a weather condition supporting cold-event occurrences, which are more likely to trigger cold disasters in the TS.

In the winter of 2008, exceptionally cold water affect the southern TS and hit the marine natural resources around the Penghu Islands in the southwestern TS, causing considerable damage in marine aquaculture; this phenomenon is hereafter

20   referred to as "cold damage". Cold sea temperatures below the critical minimum for fish could lead to a high rate of fish deaths (Hsieh et al. 2008). The death of wild fish was at least 73 t, and 80% of cage aquaculture fish were damaged (Chang et al. 2013). Chang et al. (2009) used satellite SST images around the Penghu Islands to show that the minimum SST (12.6 °C) in February 2008 was lower than the February climatological temperature (20 °C). The strong northeast monsoon in the winter of 2008, associated with La Niña, may drive the cold China Coastal Current to intrude more southward into the

25   southern TS and can even suppress the northward warm Kuroshio Branch Current intruding the TS (Chen et al. 2010; Lee et al. 2014). Liao et al. (2013) suggested that the cold damage in 2008 can be divided into three stages: First, the branch of the China Coastal Current moved cold water from the western strait to the central strait; then, a strong northeast wind intensified the southwest current; and finally, cold water gradually retreated to the north due to weakened wind.

Previous studies have revealed one single case of cold damage in the southern TS. Specifically, according to the 2012

30   newsletter by the Fisheries Research Institute of Taiwan, cold damage around the Penghu Islands has occurred three times: 2000, 2008, and 2011. The cold damage in 2008 is among the most serious events occurring in the Penghu Islands. Thus, reducing the negative consequences of damage is a major concern. Although numerous studies on the single event of cold damage in 2008 have been performed using satellite-observed data and numerical models, there is no operational system for rapidly transmitting current information on potential sea threats to mariculturists or citizens at large. The main purposes of

the current study were to clarify the predictability of cold events, that might trigger cold damage in the TS, and to present a feasible warning system with respect to marine hazards around the Penghu Islands.

2 Data and methods

The optimum interpolation daily SST dataset from the National Oceanic and Atmospheric Administration are calculated
5   from blended analyses, which is derived by combining multi-satellite data, ship observations, and buoy data (Reynolds et al. 2007). The dataset is averaged onto a 1/4° × 1/4° spatial grid and covers the period from 1981 to the present; however the current study used only the data from January 1995 to May 2017. We focused on the SST variability across the southern TS, and we confined the analysis to the 60 coldest days of winter based on the climatologically averaged SST (January 6–March 6 in non-leap years, and January 6–March 5 in leap years). During these climatologically coldest days of winter, further
10   cooling days may be expected to have the greatest implications for health and aquaculture.

The Oceanic Niño Index (ONI), defined as a 3-month running mean of SST anomalies in the region of 5°N–5°S and 120°W– 170°W, is used for classifying the ENSO cycle into El Niño (ONI ≥ 0.5 °C) and La Niña (ONI ≤ −0.5 °C) (Huang et al. 2015). In addition, the daily surface wind fields used in this study were derived from the National Centers for Environmental Prediction global analyses at 2.5° spatial resolution and can be applied from 1980 to the present, which were downloaded
15   from https://www.esrl.noaa.gov/psd/data/gridded/data.ncep.html.

3 Cold events

The current study focused on hindcasting the occurrence of low SST anomalies (SSTAs) during the 60 coldest days of winter (hereafter referred to as just "winter days"). To obtain a quantity representative of the magnitude of low SST, we calculated the SSTAs deviating from the daily climatological average and spatially averaged the SSTAs across the southern TS (the
20   blue dotted quadrilateral in Figure 1). Figure 2 shows the time series of SSTAs and highlights the SSTAs for the winter days (dots in Fig. 2a) from 1995 to 2017. During these winter days, further cooling days may be expected to have the greatest implications for health and aquaculture (hereafter referred to "cold water days"), which were defined as those whose SSTAs was lower than 1.6 times the standard deviation (approximately 95% interval of normal distribution) below the mean (i.e., −2.0 °C). Moreover, two or more consecutive cold water days were grouped into cold events; if any cold events were less
25   than 4 days apart, they were grouped into a same event. According to these definitions, 1,320 winter days of the study period, 107 cold water days and a total of 9 cold events (triangles in Fig. 2) were observed. All of the cold events revealed using the SSTAs were determined to occur during the La Niña events (Fig. 2b). Furthermore, the cold phase peak for ONI tends to occur toward the end of the calendar year and a lag correlation reflects the cold events in January–February after the peak ENSO. A lag-0- to lag-6-month correlation between rainfall anomalies in western Pacific and the peak La Niña was also
30   observed by Wang et al. (2000).

To clarify the interannual variability of cold events in the southern TS, we performed composite analyses of SST and surface wind fields for the winter days from 1995 to 2017. The spatial pattern of the long-term average for winter days was observed

to show a moderate SST belt extending from southwest to northeast, and an isotherm of nearly 18 °C across the northern Penghu Islands was revealed to separate the colder water in the west from the warmer water in the southeastern TS (Fig. 3a). The cold-water China Coastal Current flows southwestward along the coast of China and meets the warm-water northward Kuroshio Branch Current near the Penghu Islands, forming a strong sea temperature front. The SST variability is obviously

5 affected by the delicate balance between the southward China Coastal Current and the northward Kuroshio Branch Current, both of which are associated with the magnitude of the northeast monsoon (Kuo and Ho 2004). Wind fields around Taiwan are strictly dominated by the East Asian monsoons. Wind data derived from weather stations across the TS (Jan et al. 2006) showed that a northeast monsoon occurs from September to the following May and that a southwest monsoon occurs during the rest of the year. During the winter days, the northeast monsoon dominates the environmental conditions around Taiwan

10 (Fig. 3d), which illustrates it can drive the cold SST front into the southern TS.

Figure 3b, c shows the SSTA relative to the long-term average for the winter days. The SST across the TS was observed to get warmer along the China coast (Fig. 3b) when the northeast monsoon was weakened during the El Niño events, thus resulting in the wind anomaly fields illustrating southwest wind (Fig. 3e). By contrast, a negative SSTA was shown to dominate all of the TS and to expand into the southern Penghu Islands during the La Niña events (Fig. 3c). The lowest

15 anomaly was approximately −0.6 °C near the central TS. In addition, a positive anomaly regarding northeast wind was observed (Fig. 3f), which may intensify the northeast monsoon. The stronger wind generating turbulence mixing would likely lead to increased air–sea heat fluxes and would substantially affect the extent of cold water in the TS. These results imply that the SST variability in the TS is strongly associated with the ENSO cycle. Given the environmental conditions, exceptionally cold water is more likely to affect the southern TS and trigger cold damage during La Niña than during El

20 Niño events.

According to above results we summarize two possible physical mechanisms for triggering cold events in the TS. One is the balance between the southward China Coastal Current and the northward Kuroshio Branch Current, and the other one is local wind-driven entrainment. However, both processes are associated with the magnitude of wind. During the La Niña events (Fig. 4), a northeast monsoon dominates the environmental conditions around the TS with strong wind stresses. The

25 cold China Coastal Current will have more chance to intrude into the southern TS and the warm Kuroshio Branch Current will even be suppressed by strong southwestward winds. In addition, strong wind stresses can drive turbulence mixing and enhance air-sea interaction to further cool the sea water across most of the TS. Therefore, ONI and local wind speed are used as prognostic indexes to find the cold days in the following study.

4 Predictability of cold events

30 ### 4.1 Predicting by ONI

The results of the preceding analysis identify a significant correlation between cold water days and La Niña events. The association between them can be through the increased wind stress of the northeast monsoon, which may intensify the

southwestward cold current. We extended this study by understanding the relationship with monthly ONI and evaluating the prediction skill as a function of lead time.

In this study, we primarily experiment with two-class prediction problems. The ENSO cycle was quantified using the ONI, and cold water days were predicted based on the ONI falling below a threshold. There are subsequently four possible results

5   from the binary classification test: (1) the outcome predicted a cold water day is identical to the actual value (true positive, TP); however, (2) if the actual value is not a cold water day, it is classed as a false positive (FP). Conversely, (3) a true negative (TN) has been found while both the prediction state and the actual state are not cold water days; (4) the outcome predicted no cold water day is exactly opposite to the actual value (false negative, FN). For the following evaluations, an ONI −0.9 was set as the threshold, and lead days were counted ahead of the cold day. For predictions at a 90-day lead time,

10 ONI values below the threshold can be considered to correspond to the probability of cold water days occurring with a true positive rate (TPR, hit rate) of 72% and a false positive rate (FPR, false alarm rate) of 15% (the arrow in Fig. 5a). The hit rate is defined as $\sum TP / [\sum TP + \sum FN]$ (i.e. the percentage of cold water days which are correctly identified as having the condition), and false alarm rate is calculated as $\sum FP / [\sum FP + \sum TN]$. In addition, we could examine the suitability of a threshold at a special lead time by an odds ratio, defined as $[TPR(1-FPR)] / [FPR(1-TPR)]$. In the above case, the odds ratio

15 was 14.8, which implies the probability of correct predictions are almost a 15-fold increase (the arrow in Fig. 5b).

Depending on the tolerance for the TPR and FPR, the choice of threshold for a prediction can be varied; more negative ONI thresholds reduce both the TPR and FPR. This trade-off is presented by relative operating characteristic (ROC) curves (Hanley and McNeil 1982) that represent the relationship between the TPR and FPR as a function of threshold (Fig. 5a). ROC curves are quantified by integrating the area under the curve, called ROC score or AUC. The score is used as the proxy

20 throughout the analysis because it is appropriate for assessing unusual events (Stephenson et al. 2008; McKinnon et al. 2016). When a ROC score is higher, it would be a more discriminating prediction method. In this study, the skill of the ONI-based prediction was shown to peak at a lead time of 60 days, with an ROC score of 0.78, and generally decreased with increasing lead time. Moreover, significance can be estimated through the creation of a null distribution of the quantity of interest by using a block bootstrap (McKinnon et al. 2016), and significant results above the 95% confidence level are presented

25 throughout this article. An ROC score greater than or equal to 0.6 is designated to be significant for predictions of cold water days. As shown in Fig. 5a, ROC scores decreased with lead time and were no longer significant by a lead time of 240 days. Notably, the ONI was estimated according to the 3-month running mean of monthly SSTAs; in other words, the latest ONI value obtainable in December is the value for October. Hence, the ONI-based prediction of cold water days can actually be employed with a lead time of 0–150 days. For simplicity, we still used the time of the ONI ahead of the cold day to describe

30 the lead time in the subsequent analysis.

4.2 Predicting by wind

The relationship between wind stress and cold water can be understood through local wind-driven entrainment, whereby a strong La Niña episode results in an enhanced winter monsoon and strong wind stress increases turbulent mixing in favor of heat fluxes.

5 We next focused on the relationship between wind speed and the probability of cold water days. Wind speed variability across the TS could be quantified using an integrated wind speed (IWS) over a pre-specified period. The IWS was calculated using integration periods of 1 to 30 days, and the correlation coefficients between IWS and SSTAs are shown in Fig. 6a. The 10-day integration period was observed to have the highest correlation with the SSTA variability, and the correlation coefficient was approximately –0.43 (p < 0.05). Therefore, we focused on the IWS with a running integration period of 10

10 days in the subsequent analysis. Figure 6b shows the water temperature to drop following a stronger IWS.

As indicated by the ROC curves, the wind-based prediction had an ROC score of 0.8 at a lead time of 0 days, which is counted following the last day over which wind speed is integrated (Fig. 7). This result is consistent with the expected relationship between wind speed and sensible cooling. The wind-based predictions were observed to have significant prediction skill for lead times from 0 to 30 days (ROC score ≥ 0.6), and the prediction skill generally decreased with

15 increasing lead time. For predictions at a 15-day lead time, the highest odds ratio (6.0) was determined using a threshold of 115 m/s. An IWS below the special threshold was determined to correspond to the occurrence of cold water days with a TPR of 78% and an FPR of 38%.

5 Warning mechanism for Penghu Islands

According to the analysis of predictability presented in the preceding section, cold water days can be predicted using the

20 ONI for a long-lead prediction (60–210 days) and the IWS for middle- to short-lead predictions (0–30 days). We established a warning mechanism based on the ONI and IWS. The ONI-based prediction was employed to predict cold water days at a lead time of around 90 days. Hence, the ONI of –0.9, which engendering the highest accuracy (0.78) and odds ratio (14.8), was selected as the threshold. Moreover, the IWS-based prediction was employed for middle- and short-lead predictions. As shown in Fig. 8, the ROC scores varied with the integration periods and lead time. The prediction conducted at a lead time of

25 around 15 days and integration period of 10 days had an ROC score of approximately 0.74. The threshold was set at 115 m/s because this was observed to result in the highest accuracy (0.70) and odds ratio (6.0). In addition, the prediction conducted at a lead time of around 5 days and integration periods of around 20 days had higher ROC scores compared with those conducted at other integration periods. Regarding the prediction of cold water days at an integration period of 20 days, the prediction conducted with a threshold of 250 m/s had an accuracy of 0.76. Therefore, a warning mechanism could be

30 established based on this analysis (Table 1).

6 Hindcasting cold water days

A hindcast of cold water days over the period 1995–2017 (Fig. 9) was obtained by using the warning mechanism in Table 1. The results clearly demonstrate high-risk warnings for the winters of 2000, 2008, 2011, and 2012. By monitoring the number of fish deaths around the Penghu Islands, Lu et al. (2012) reported finding a large number of dead farmed fish in

5   exceptionally cold water in the winters of 2000, 2008, and 2011. This agrees with the periods of high risk identified by this warning mechanism.

To illustrate specific predictions that could be made using the warning mechanism, we conducted a case study for the winter of 2011. Figure 10 displays the developing process of a cold water event from six satellite SST maps. Before the occurrence of the cold water event, the SST in the TS was 16 °C (Fig. 10a). An obvious cold front crossed from the Taiwan bank to the

10 Chang-Yuen ridge and approached the Penghu Islands. Cold water (approximately 14 °C) developed along the coast of China on January 29, 2011 (Fig. 10b), and it extended to the southern TS afterward (Fig. 10c, d). When the exceptionally cold water intruded into the southern TS, the Penghu Islands were surrounded by extremely cold water below 16 °C. Finally, at the end of the cold event, warmer water above 22 °C was re-established through the channel to the east of Penghu Islands (Fig. 10e, f), and the cold water gradually retreated to the north due to the weakening wind (Fig. 10g). Moreover, to examine

15 satellite SST, buoy measurements of SST provided by the Central Weather Bureau of Taiwan (red star in Fig. 10a) were used. Although the satellite SST is overall higher than that measured by the buoy, Fig. 10g shows the variations in both SST measurements to be largely consistent. In addition, the SST variability was observed to be associated with the 10-day IWS. When the IWS remained at approximately 140 m/s from January 10, the SST kept decreasing to approximately 14 °C until the IWS decreased on February 2. After wind speed weakening, the SST around the Penghu Islands rose immediately, which

20 agrees with the sequence of SST maps shown in Fig. 10d–f. A similar process was observed in the other cold events of 2000, 2008, and 2012.

Buoy SST measurements provide a means for examining the applicability of the warning mechanism. The buoy sited on the north of Penghu Islands measures SST from January 2007 to the present. The observational period includes three extremely cold winters whose warning level reached high risk: 2008, 2011, and 2012. Winter 2008 has the severest cold event over the

25 past decade, and the minimum SST (approximately 11 °C) broke the record temperature (a fact discussed in numerous previous studies; e.g., Chen et al. 2010; Liao et al. 2013; Lee et al. 2014). Through the application of the warning mechanism, the hindcast of the 2008 winter showed that a high-risk warning could precede the coldest water day by 19 days (Fig. 11a); similarly, the high-risk warnings for 2011 and 2012 could lead by 22 and 21 days, respectively. The lowest SST was just 16 °C in the winter of 2012, whereas the SST was lower than the standard deviation of the climatological average (yellow

30 shading in Fig. 11), which is cold enough to induced the death of caged fish around Penghu Islands (Chang et al. 2013). Notably, the SST variability over an approximately 10-day period in February 2012 might be dominated by a sub-mesoscale process, which agrees with the higher correlation between the SST and 10-day IWS in Fig. 6a.

7 Summary

We used optimum interpolation SST data to identify exceptionally cold water over the southern TS during the period 1995–2017. The results reveal a total of 107 cold water days and 9 cold events likely to trigger cold disasters in the TS. Cold water develops along the coast of China and extends to the southern TS with sustained strong winds. In addition, these

5   exceptionally cold water days always occur during La Niña events, and climatological maps show that the SST and wind speed over the TS are extremely low and strong in La Niña winters compared with normal or El Niño winters. A correlation was also obtained for SSTAs and 10-day IWS, with a correlation coefficient of −0.43 (p < 0.05).

According to the results associated with ENSO and wind speed, the predictability of cold water days can be estimated by ROC curves; when ROC scores were higher than or equal to 0.6, methodologies based on the ONI or 10-day IWS were

10   observed to be significant (above the 95% confidence level) for predictions of cold water days. The ONI- and IWS-based predictions could be conducted at lead times of 60–210 and 0–30 days, respectively. Given this predictability, a possible warning mechanism based on the ONI and IWS was established. In this mechanism, if the monthly ONI is lower than or equal to −0.9, a cyan warning light indicating required action is triggered; This light turns yellow if the 10-day IWS is stronger than or equal to 115 m/s, meaning a moderate risk of exceptionally cold water. Red light signaling high risk displays

15   when the 20-day IWS is greater than or equal to 250 m/s. After the application of the warning mechanism, a hindcast of cold water days over the period 1995–2017 revealed four winters with a high risk of cold damage (2000, 2008, 2011, and 2012). The warning mechanism evidently fulfills the requirements of the recently developed methodology of early warning systems for weather-related hazards, as implemented by the Central Weather Bureau of Taiwan. Warning lights based on the ONI and IWS indicate characteristics of exceptionally cold water affecting the Penghu Islands, and they thus facilitate identifying

20   possible periods of exposure to extremely cold water. The warnings thus generated can be sent in an efficient and timely manner to mariculturists.

Acknowledge

NCEP Daily Global Analyses data provided by the NOAA/OAR/ESRL PSD, Boulder, Colorado, USA, from their Web site

25   at http://www.esrl.noaa.gov/psd/. This work was supported by the Central Weather Bureau, Taiwan, through grant 1062076C and the National Natural Science Foundation of China (U1405233).

References

Alexander M, Scott J (2002) The influence of ENSO on air-sea interaction in the Atlantic. Geophys Res Lett 29:46-41-46-44 doi:10.1029/2001GL014347

30   Chang Y, Lee K-T, Lee M-A, Lan K-W (2009) Satellite Observation on the Exceptional Intrusion of Cold Water in the Taiwan Strait. Terr Atmos Ocean Sci 20:661-669 doi:10.3319/TAO.2008.08.07.01

Chang Y, Lee M-A, Lee K-T, Shao K-T (2013) Adaptation of fisheries and mariculture management to extreme oceanic environmental changes and climate variability in Taiwan. Marine Policy 38:476-482 doi:10.1016/j.marpol.2012.08.002

Chen C-TA, Jan S, Huang T-H, Tseng Y-H (2010) Spring of no Kuroshio intrusion in the southern Taiwan Strait. J Geophys Res Oceans 115 doi:10.1029/2009JC005804

5   Chen H-W et al. (2016) Temporal variations of volume transport through the Taiwan Strait, as identified by three-year measurements. Cont Shelf Res 114:41-53 doi:10.1016/j.csr.2015.12.010

Hanley JA, McNeil BJ (1982) The meaning and use of the area under a receiver operating characteristic (ROC) curve. Radiology 143:29-36 doi:10.1148/radiology.143.1.7063747

Hsieh H, Hsien Y-L, Jeng M-S, Tsai W-S, Su W-C, Chen C (2008) Tropical fishes killed by the cold. Coral reefs 27:599-599

10   doi:10.1007/s00338-008-0378-3

Huang B et al. (2015) Extended reconstructed sea surface temperature version 4 (ERSST. v4). Part I: upgrades and intercomparisons. J Climate 28:911-930 doi:10.1175/JCLI-D-14-00006.1

Jan S, Sheu DD, Kuo H-M (2006) Water mass and throughflow transport variability in the Taiwan Strait. J Geophys Res Oceans 111 doi:10.1029/2006JC003656

15   Jan S, Wang J, Chern C-S, Chao S-Y (2002) Seasonal variation of the circulation in the Taiwan Strait. J Marine Syst 35:249-268 doi:10.1016/S0924-7963(02)00130-6

Kuo N-J, Ho C-R (2004) ENSO effect on the sea surface wind and sea surface temperature in the Taiwan Strait. Geophys Res Lett 31 doi:10.1029/2004GL020303

Lau N-C, Nath MJ (2006) ENSO modulation of the interannual and intraseasonal variability of the East Asian monsoon-A

20   model study. J Climate 19:4508-4530 doi:10.1175/JCLI3878.1

Lee M, Yang Y, Shen Y, Chang Y, Tsai W, Lan K, Kuo Y (2014) Effects of an unusual cold-water intrusion in 2008 on the Catch of Coastal Fishing Methods around Penghu Islands, Taiwan. Terr Atmos Ocean Sci doi:10.3319/TAO.2013.08.06.01

Liao E, Jiang Y, Li L, Hong H, Yan X (2013) The cause of the 2008 cold disaster in the Taiwan Strait. Ocean Modelling 62:1-10 doi:10.1016/j.ocemod.2012.11.004

25   Lu Yi-Lin, Hsien I-L, Chung C-S, Lin, C-Y, Chen S-C, Tsai W-S (2012) Aquaculture management during a cold spell in the Penghu Islands. Newsletter of Fisheries Research Institute (in Chinese) 37: 21-25

McKinnon KA, Rhines A, Tingley MP, Huybers P (2016) Long-lead predictions of eastern United States hot days from Pacific sea surface temperatures. Nature Geosci 9:389-394 doi:10.1038/ngeo2687

McPhaden MJ, Zebiak SE, Glantz MH (2006) ENSO as an Integrating Concept in Earth Science. Science 314:1740-1745

30   doi:10.1126/science.1132588

Mora C, Ospina A (2002) Experimental effect of cold, La Nina temperatures on the survival of reef fishes from Gorgona Island (eastern Pacific Ocean). Marine Biology 141:789-793 doi:10.1007/s00227-002-0862-1

Philippon N, Rouault M, Richard Y, Favre A (2012) The influence of ENSO on winter rainfall in South Africa. Int J Climatol 32:2333-2347 doi:10.1002/joc.3403

Reynolds RW, Smith TM, Liu C, Chelton DB, Casey KS, Schlax MG (2007) Daily high-resolution-blended analyses for sea surface temperature. J Climate 20:5473-5496 doi:10.1175/2007JCLI1824.1

Shang S, Zhang C, Hong H, Liu Q, Wong GTF, Hu C, Huang B (2005) Hydrographic and biological changes in the Taiwan Strait during the 1997–1998 El Niño winter. Geophys Res Lett 32:n/a-n/a doi:10.1029/2005GL022578

5   Stephenson DB, Casati B, Ferro CAT, Wilson CA (2008) The extreme dependency score: a non-vanishing measure for forecasts of rare events. Meteorol Appl 15:41-50 doi:10.1002/met.53

Ustrnul Z, Wypych A, Henek E, Maciejewski M, Bochenek B (2015) Climatologically based warning system against meteorological hazards and weather extremes: the example for Poland. Natural Hazards 77:1711-1729 doi:10.1007/s11069-015-1673-2

10   Wang B, Wu R, Fu X (2000) Pacific–East Asian teleconnection: how does ENSO affect East Asian climate? J Climate 13:1517-1536 doi:10.1175/1520-0442(2000)013<1517:PEATHD>2.0.CO;2

Wu C-R, Chao S-Y, Hsu C (2007) Transient, seasonal and interannual variability of the Taiwan Strait current. J Oceanogr 63:821-833 doi:10.1007/s10872-007-0070-1

Zhang W, Zhuang X, Chen CA, Huang T (2015) The impact of Kuroshio water on the source water of the southeastern
15   Taiwan Strait: numerical results. Acta Oceanologica Sinica 34:23-34 doi:10.1007/s13131-015-0720-x
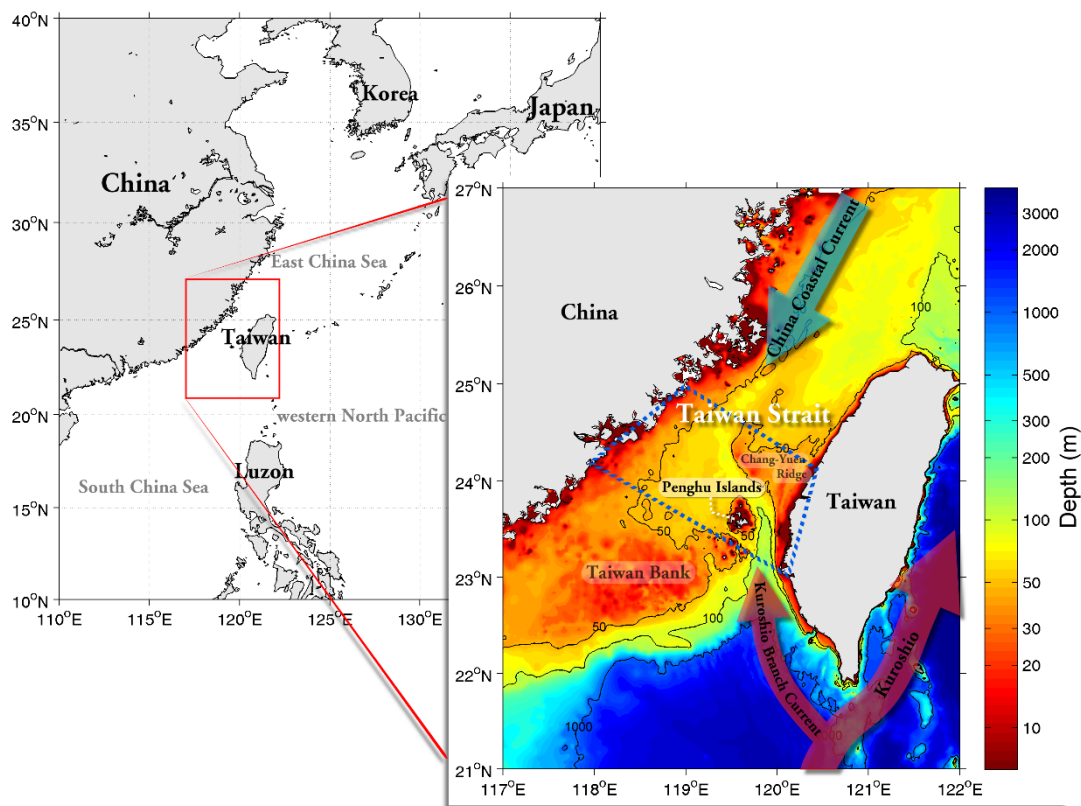
Figure 1: Bathymetric chart (shaded color) and sketches of the China Coastal Current, Kuroshio, and Kuroshio Branch Current.
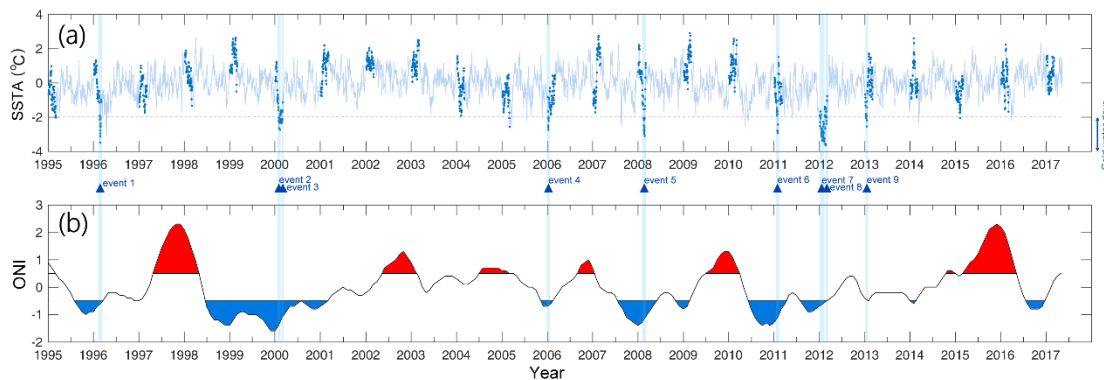
5 **Figure 2: (a) Time series of SSTAs (shading line) and that during the winter days are highlighted in dots. The dashed line denotes a magnitude of 1.6 times the standard deviation below the mean SSTA. (b) ONI time series within January 1995 and May 2017. Positive anomalies (≥0.5 °C, shaded red) indicate El Niño events, and negative anomalies (≤−0.5 °C, shaded blue) indicate La Niña events. Blue bars and triangles denote the occurrences of cold events.**
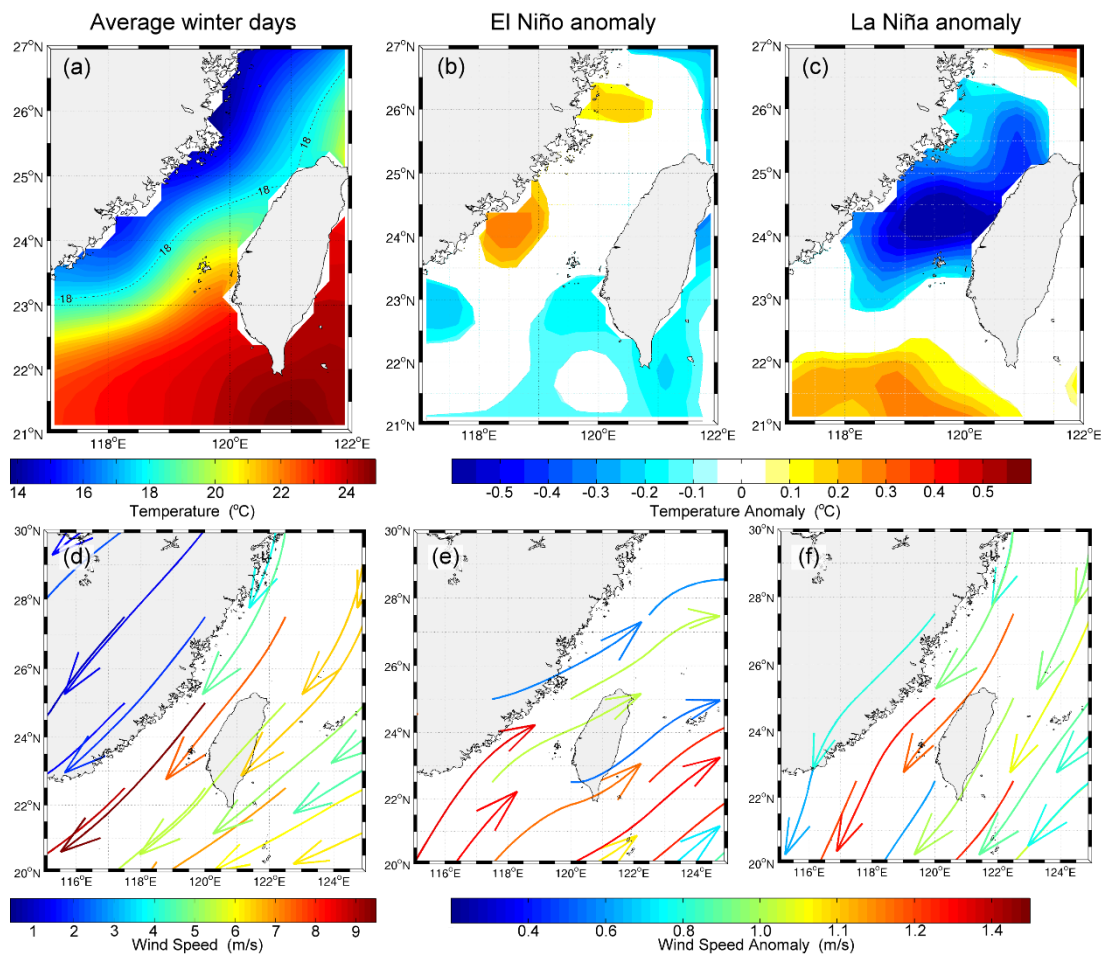
Figure 3: Composite of SST (a to c) and surface wind fields (d to f) for (a, d) average winter days, (b, e) El Niño anomaly, and (c, f) La Niña anomaly. Only anomalies above the 95% confidence level are shown.
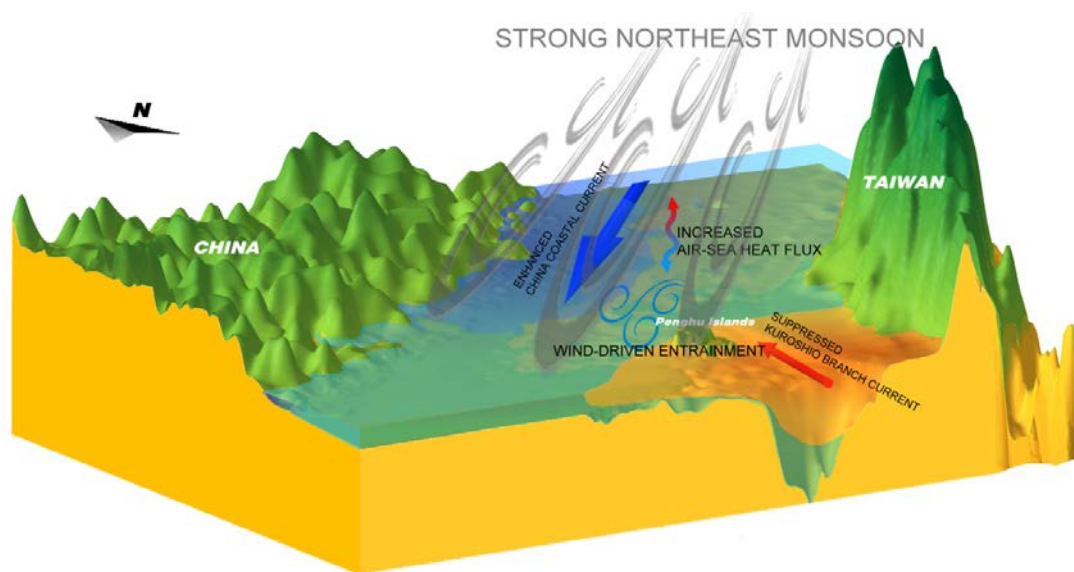
Figure 4: A cold-event sketch during La Niña events.
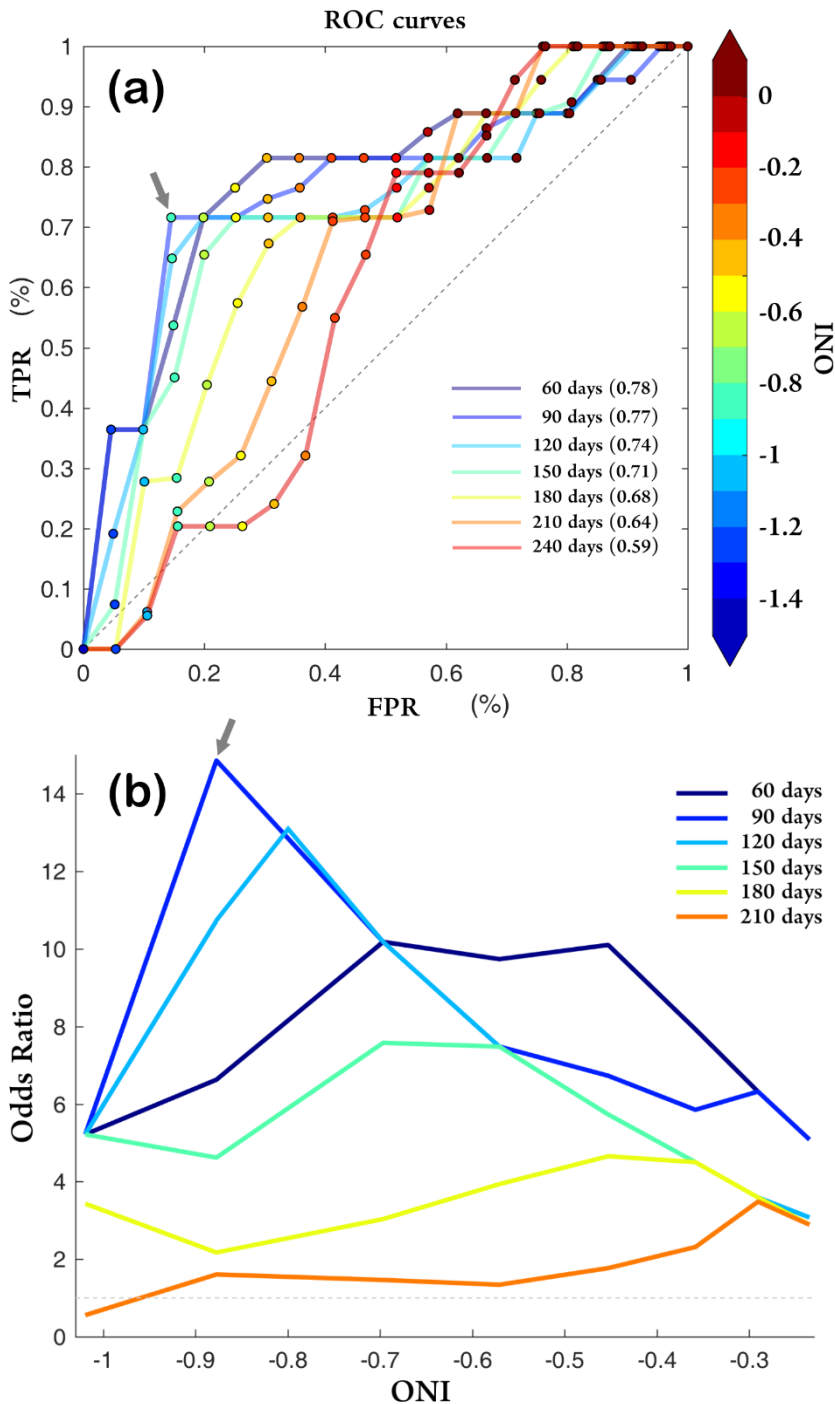
Figure 5: (a) ROC curves for predicting cold water days at lead times of 60, 90, 120, 150, 180, 210, and 240 days using the negative ONI. Numbers in parentheses in the legend are ROC scores for each lead time. The thresholds used to calculate TPRs and FPRs are showed from the 100th (lower left squares) to the 0th (upper right squares) percentile of negative ONI in decrements of 5%.

5 **ONIs at the dots are indexed by the colorbar. ROC scores ≥ 0.6 indicate a significant (p < 0.05) proxy for predictability. (b) Odds**

ratios vary with ONI thresholds at lead times of 60, 90, 120, 150, 180, 210, and 240 days. Arrows denote the point with a -0.9 threshold at a 90-day lead time.
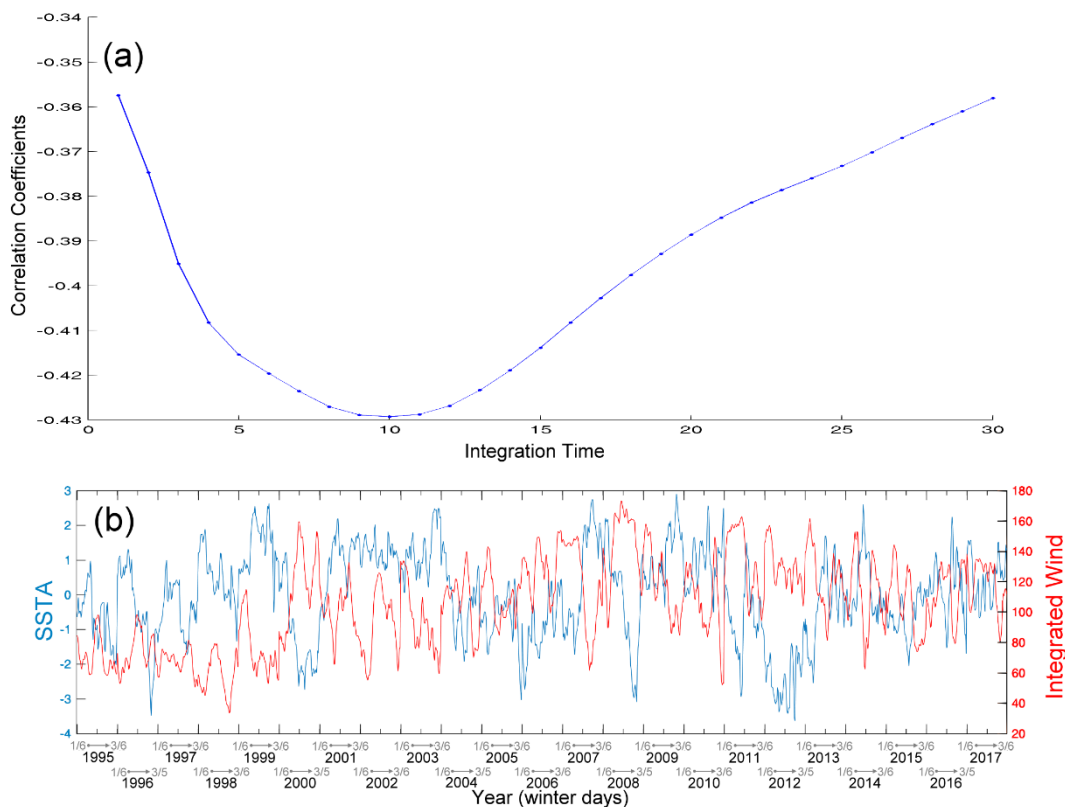
Figure 6: (a) Correlation coefficients varied with integration time. (b) Time series of SSTAs for the winter days and IWS with an integration time of 10 days.
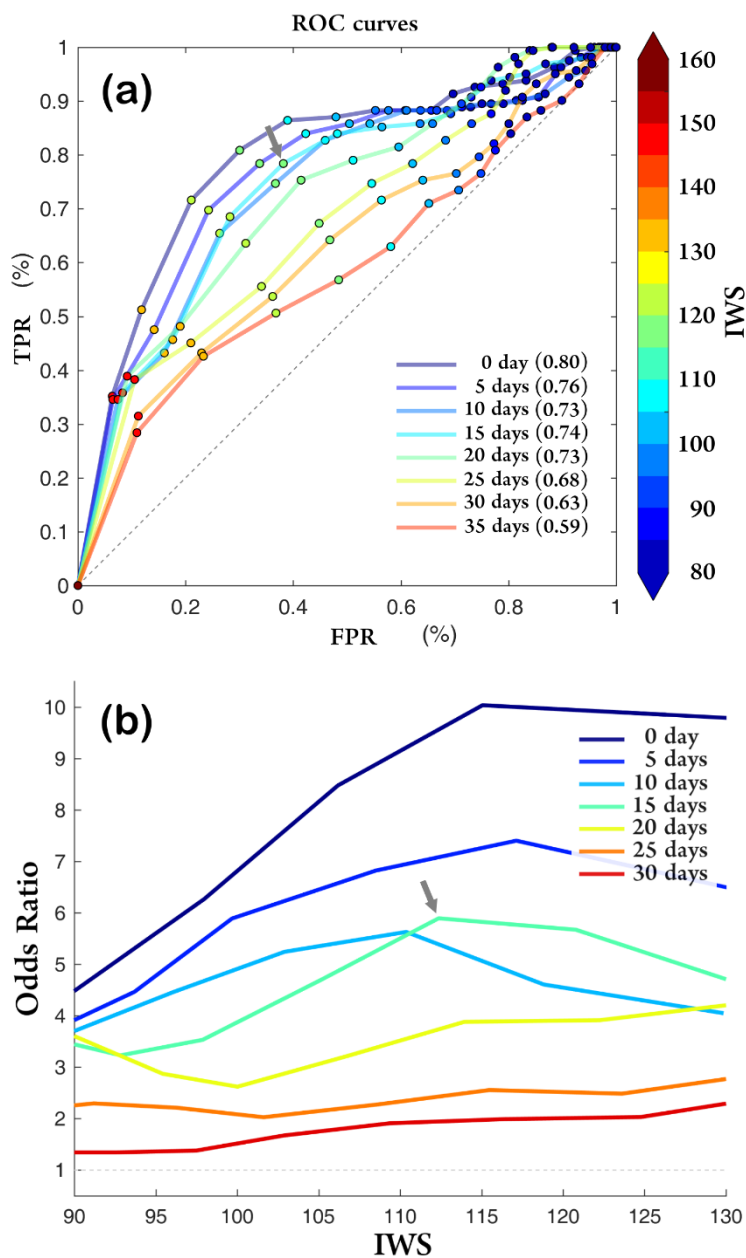
Figure 7: As in Fig. 5, but for predictions of cold events at lead times of 0, 5, 10, 15, 20, 25, 30, and 35 days using the wind speed with an integration time of 10 days. Arrows denote the point with a 115-m/s threshold at a 15-day lead time.
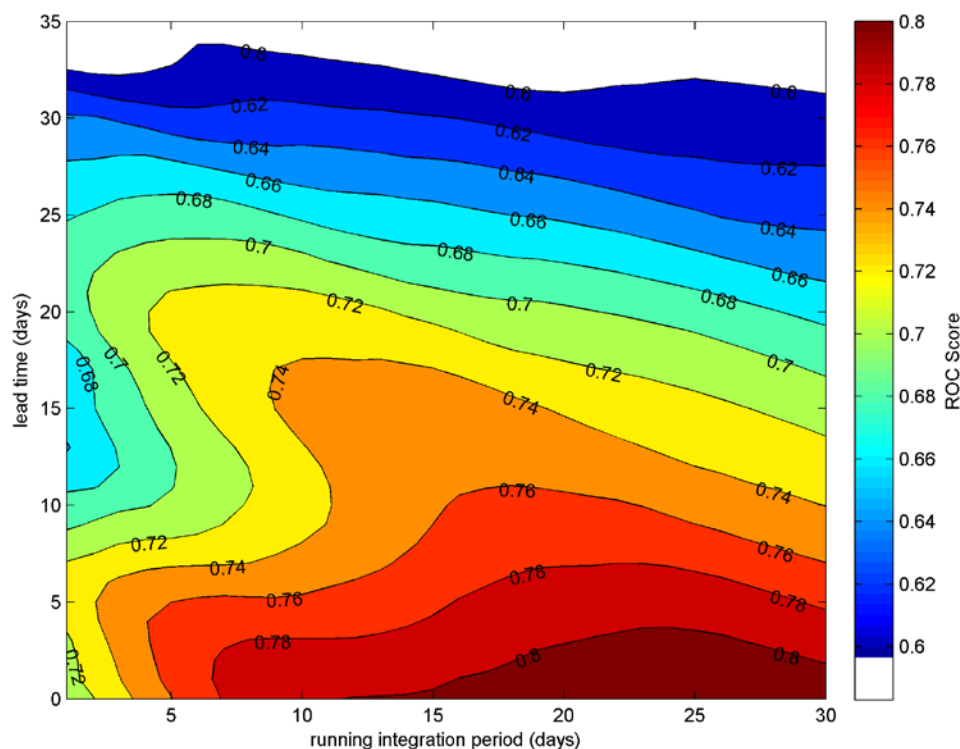
Figure 8: ROC score diagram of IWS-based prediction. The white color masks nonsignificant regions, where ROC scores are below the 95% confidence level.
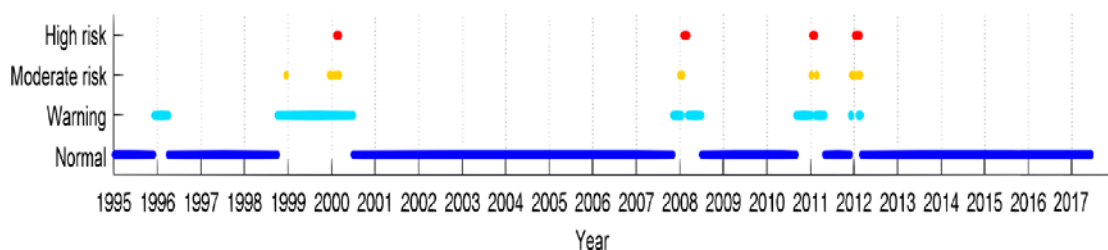
5   **Figure 9: Warning lights of cold water days for Penghu Islands.**
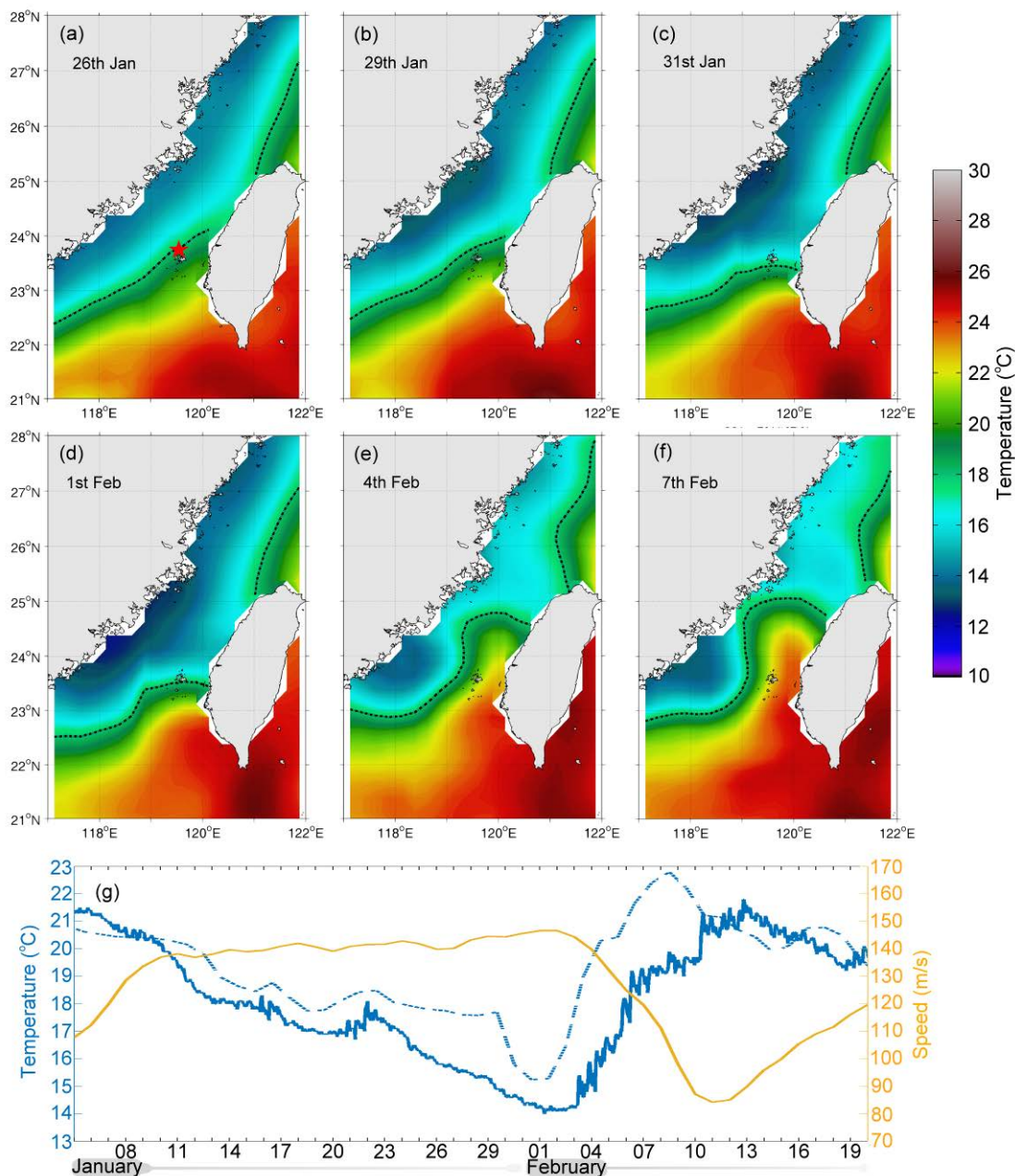
Figure 10: Cold event in the winter of 2011. (a to f) A map sequence of satellite SST. The red star indicates the position of the buoy from the Central Weather Bureau of Taiwan. Dashed lines are isotherm lines of 18 °C. (g) Time series of satellite SST (blue dashed line), buoy SST (blue line), and 10-day IWS (yellow line) on the red star location from January 5 to February 20.
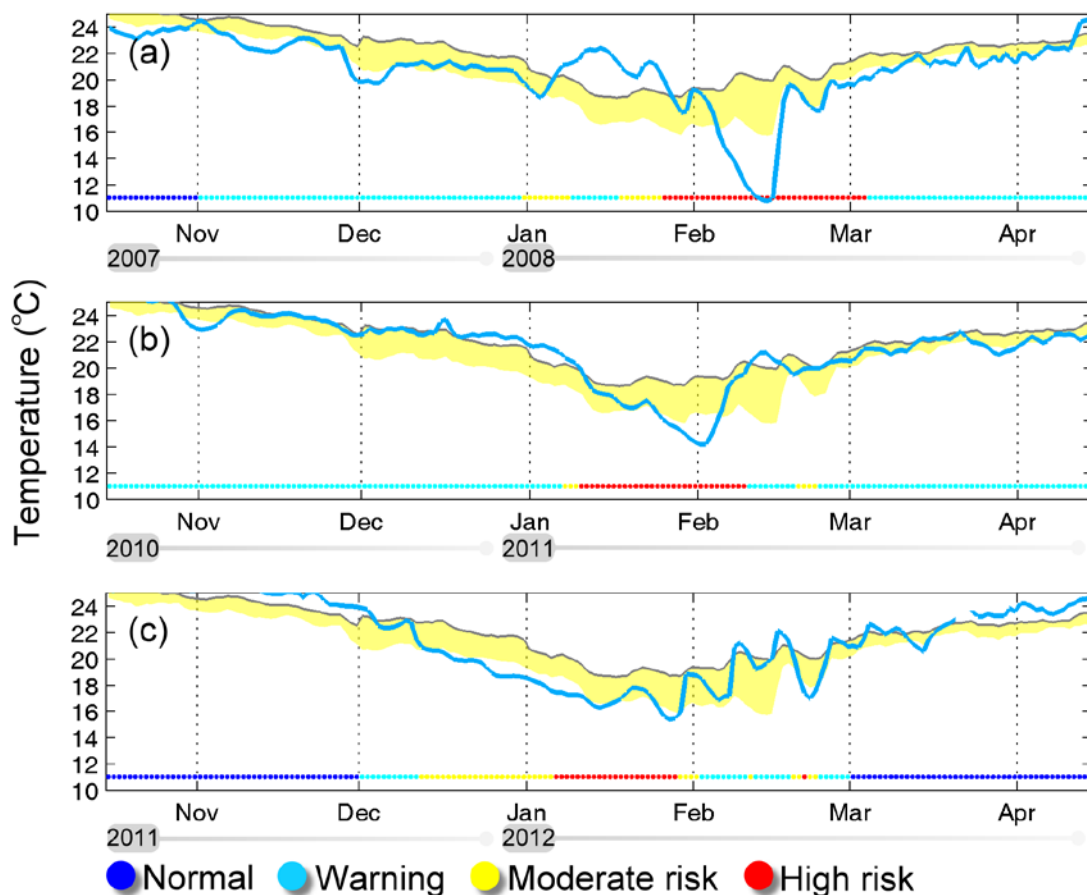
Figure 11: Cold events in (a) 2008, (b) 2011, and (c) 2012. Blue line: buoy measurements of SST; gray line: 10-year climatological average; yellow shading: range of standard deviation below the average. Color dots are warning lights.

Table 1: Warning thresholds suggested for exceptionally cold water days

Type	Conditions	Possible Occurrence Time
Warning	ONI ≤ -0.9	around the next 90 days (30 days[a])
Moderate risk	10-day IWS ≥ 115	around the next 15 days
High risk	20-day IWS ≥ 250	around the next 5 days

[a] real time lead time considering when the ONI value can be obtained.